IEEE Access
Multidisciplinary | Rapid Review | Open Access Journal

Received October 2, 2019, accepted November 5, 2019, date of publication November 12, 2019, date of current version November 27, 2019.

Digital Object Identifier 10.1109/ACCESS.2019.2953122

Demonstration-Guided Pose Planning and Tracking for Multi-Section Continuum Robots Considering Robot Dynamics

IBRAHIM A. SELEEM[1,4], SAMY F. M. ASSAL[1,5], HIROYUKI ISHII[2], AND HAITHAM EL-HUSSIENY[3]

[1]Mechatronics and Robotics Engineering Department, School of Innovative Design Engineering, Egypt-Japan University of Science and Technology, New Borg El-Arab 21934, Egypt
[2]Faculty of Science and Engineering, Waseda University, Tokyo 169-8050, Japan
[3]Electrical Engineering Department, Faculty of Engineering at Shoubra, Benha University, Benha 13511, Egypt
[4]*(On leave)* Department of Industrial Electronics and Control Engineering, Faculty of Electronic Engineering, Menoufia University, Shibin el Kom 32952, Egypt
[5]*(On leave)* Department of Production Engineering and Mechanical Design, Faculty of Engineering, Tanta University, Tanta 31527, Egypt

Corresponding author: Ibrahim A. Seleem (ibrahim.seleem@ejust.edu.eg)

This work was supported by the Mission Department of the Ministry of Higher Education (MOHE) of Egypt for granting him scholarship to carry out his graduate studies with the Egypt-Japan University of Science and Technology.

ABSTRACT Recently, there has been an increased interest in the deployment of continuum robots in unstructured and challenging environments. However, the application of the state-of-the-art motion planning strategies, that have been developed for rigid robots, could be challenging in continuum robots. This, in fact, is due to the compliance that continuum robots possess besides their increased number of degrees of freedom. In this paper, a Demonstration Guided Pose Planning (DGPP) technique is proposed to learn and subsequently plan for spatial point-to-point motions for multi-section continuum robots. Motion demonstrations, including position and orientation, are collected from a human via a flexible input interface that is developed to command the continuum robot intuitively via teleoperation. A dynamic model based on Euler-Lagrange formalism is derived for a two-section continuum robot to be considered while planning for the robot motions. Meanwhile, a Proportional-Derivative (PD) computed torque controller with a Model Reference Adaptive Kinematic Control (MRAKC) scheme are developed to ensure the tracking performance against system uncertainties and disturbances. Also, the system stability analysis based on Lyapunov quadratic equation is proven. Simulation results prove that the proposed DGPP approach, along with the developed control scheme, have the ability to learn, generalize and reproduce spatial motions for a two-section continuum robot while avoiding both static and dynamic obstacles that could exist in the environments.

INDEX TERMS Continuum robots, motion planning, dynamic movement primitives, kinematic control, dynamic modeling.

I. INTRODUCTION

Tremendous inspection and rescue operations have witnessed the engagement of robots in their applications that are potentially expected to grow further in the next few years [1]. Recently, inspired by the incredible capabilities of biological appendages; such as elephant trunks and octopus arms, continuum robots exhibit an impressive potential towards the exploration of narrow and confined spaces. Their continually bending flexible backbones facilitate such kind of maneuverability to shape their whole bodies to suit tight spaces [2] in contrary to rigid robots, such as in Minimally Invasive Surgeries (MIS) or nuclear decontamination. Meanwhile, from a safety perspective, the compliance of such robots enriches their applicability to safely interact close to human, for instance in wearable assistive robots [3], [4].

Despite the growth potential of continuum robot applications, planning motions for such robots could be challenging and complex. This, in particular, is due to redundant degrees of freedom especially if the robot composed of multiple flexible sections. In literature, several attempts have been made towards planning safe paths for continuum robots without taking into account their intrinsic compliance [5]. For instance, in [6], a points-based path planning (PoPP)

The associate editor coordinating the review of this manuscript and approving it for publication was Hassen Ouakad.

algorithm was introduced to plan two-dimensional motions for constant-curvature continuum robots. To improve the limitations in the existing path planning techniques, the developed PoPP technique computes the path by considering two safety parameters; namely, the step size and the minimum marginal distance. In [7], an offline motion planning technique was proposed for a two-section continuum robot based on the closed-loop Jacobian pseudo-inverse method. On the other hand, a proactive path planning approach of multi-section continuum robot was presented in [8], where a set of proximity sensors was mounted on discrete positions on the robot's backbone to safely avoid static obstacles that could exist within its environment. Other state-of-the-art motion planning approaches that are originally proposed for rigid robots, such as graphical model [9] and potential field [10] techniques, could be utilized for planning motions for continuum robots. However, these techniques mainly rely on the robot parameters that have to be identified perfectly. Otherwise, improper chosen parameters could excite the robot dynamics which could be severe in continuum robots due to their compliant behavior.

Recently, a general learning approach has been designed for teaching rigid robots from human demonstrations on how to plan and execute complex tasks [11]. In this regard, state-action pairs of the required task were recorded during the teacher's demonstrations [12], that could be collected either kinesthetically [13] or via teleoperation [14]. Satisfactory results were obtained in applying Learning from Demonstrations (LfD) approaches in different applications such as in generating the whole body dancing motions for a biped humanoid robot [15], handwriting robotic applications [16], obstacle avoidance of robotic arm [17] and mobile robots [18].

However, so far, there has been a little discussion about applying LfD approaches in planning motions for continuum robots. For instance, in [19], a motion planning technique for a multi-section flexible robot actuated by electromotive polymers was developed in planar environments while assuming static settings. The developed approach was built based on LfD with Gaussian mixture model and Gaussian Mixture Regression (GMR) for encoding the collected trajectories and generating smooth paths. However, the human operator was needed to adjust the voltage of each section using trial and error method to accomplish the task which is a time consuming process. A skill transfer of real octopus movements to a constant curvature flexible surgical robot (STIFF-FLOP) was presented in [20]. The learning skills were encoded and reproduced using Dynamic Movement Primitives (DMP) approach based on GMR which was used for learning the basis functions and force behaviors. However, the collected real octopus data was small and approximated by 7-order polynomial which may cause ignorance of the real robot dynamics. Moreover, in [21], the generated motion skills of Shape Memory Alloy (SMA)- actuated flexible robotic arm inspired by octopus arm was developed. The movements were learned based on different activation functions such as step, Gaussian and positive sine functions. However, the designed motion planning approach was too slow and the used activation functions were not generalized for the generation of primitive behaviors.

In our previous work [22], [23], a demonstration-guided path planning approach was developed for a constant curvature two-section continuum robot. The human demonstrations were collected intuitively via teleoperation of a flexible input interface to suit the structure of the continuum robot. The developed approach has addressed only the end-effector position without considering its orientation that could be necessary for different applications such as six DOF pose tracking. In addition, the developed technique assumed a kinematic-based teleoperation setting where the robot dynamic aspects, such as compliance, friction, and weight were neglected.

The contribution of this paper is twofold. First, it presents a Demonstration-Guided Pose Planning (DGPP) approach that addresses the pose of a multi-section continuum robot. The proposed DGPP approach is mainly based on human demonstrations that are collected by teleoperating the continuum robot intuitively via a flexible rod interface. Thereafter, the DMP [11] framework is applied over the demonstrated motions to generate and generalize for the desired pose while accounting for both static and dynamic obstacles that could exist within the robot's environment. The second contribution of this paper is to derive the spatial dynamic equations that describe the motion of a multi-section extensible continuum robot. The derived model is based on the Euler Lagrange formalism and aims to incorporate the robot dynamics in the proposed DGPP approach in both learning and production phases. Meanwhile, based on the derived dynamics, a Jacobian-based Model Reference Adaptive Kinematic Control (MRAKC) along with a Proportional Derivative (PD) computed torque dynamic controller are proposed to track the generated desired end-effector poses to ensure the robustness against the model inaccuracies and the external disturbances.

In the remainder of this article, the kinematics of constant curvature continuum robots is briefly reviewed in Section II, while the dynamic modeling of an extensible two-section continuum robot is derived in Section III. The proposed Demonstration-Guided Pose Planning (DGPP) approach is described in details in Section IV for both the position and the orientation of the robot. The Model Reference Adaptive Kinematic Control (MRAKC) along with a computed torque dynamic control is presented in Section V. The system stability analysis based on Lyapunov formulation is presented in Section VI. The results of evaluating the proposed DGPP and the derived dynamics-based control are presented and discussed in Section VII. Finally, the conclusion and future work are presented in Section VIII.

II. KINEMATICS OF CONTINUUM ROBOTS

Continuum robots are flexible structures that have the ability to bend smoothly through curvilinear paths by applying moment on its distal tip. Different actuation, such as

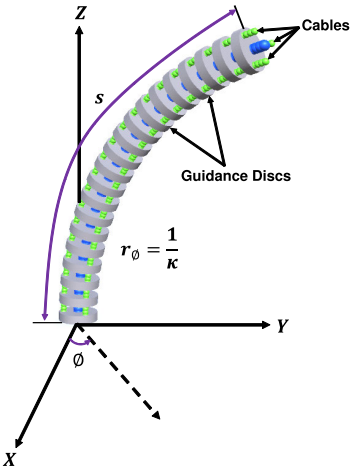

FIGURE 1. Structure of a cable-driven one-section continuum robot.

cable-driven, pneumatically-actuated and hydraulically-actuated are commonly used in continuum robots to achieve the desired tip bending. In this research paper, the cable-driven continuum robot is considered, However, applications of the proposed DGPP approach can be generalized for pneumatic-driven or hydraulically-driven continuum robots.

A. FORWARD KINEMATICS

The structure of a cable-driven continuum robot with one-section is shown in Fig. 1. The moment on the robot's tip can be adjusted by varying the respective lengths of three cables that attached to the robot's end position through guidance disks. To increase the dexterity of the robot, usually more than one section are stacked up together. The constant-curvature approach [24] is considered while deriving the forward kinematics that relates the pose of each section i to its configuration space variables; namely, the arc length s_i, curvature κ_i and the angle of curvature ϕ_i.

In this regard, the tip pose of each section i is computed with respect to its base, or the section $i-1$ tip, as follows,

$$
{}^{i-1}T_i = \begin{bmatrix}
\cos^2\phi_i(\cos(\kappa_i s_i)-1)+1 & \sin\phi_i\cos\phi_i(\cos(\kappa_i s_i)-1) & \cos\phi_i\sin(\kappa_i s_i) & \frac{\cos\phi_i(\cos(\kappa_i s_i)-1)}{\kappa_i} \\
\sin\phi_i\cos\phi_i(\cos(\kappa_i s_i)-1) & \cos^2\phi_i(1-\cos(\kappa_i s_i))+\cos(\kappa_i s_i) & -\sin\phi_i\sin(\kappa_i s_i) & \frac{\sin\phi_i(\cos(\kappa_i s_i)-1)}{\kappa_i} \\
-\cos\phi_i\sin(\kappa_i s_i) & \sin\phi_i\sin(\kappa_i s_i) & \cos(\kappa_i s_i) & \frac{\sin(\kappa_i s_i)}{\kappa_i} \\
0 & 0 & 0 & 1
\end{bmatrix} \tag{1}
$$

In continuum robots with m sections, the distal end-effector pose is computed by applying the transformation matrix in (1) along m, i.e. $\prod_{i=1}^{m} {}^{i-1}T_i$. As noted, in each element of the last column of (1), the denominator is divided by κ_i that could be close to zero when the corresponding section is stretched straight. This, in turn could cause mathematical singularity that is tackled in this research by computing the 5^{th}-order Taylor Expansion of the Cartesian tip point position $\boldsymbol{p}_i \in \mathbb{R}^3$ of each section with acceptable error for the small range of the bending angle as follows [25],

$$
\begin{aligned}
{}^{i-1}\boldsymbol{p}_i &= \begin{bmatrix} x_i \\ y_i \\ z_i \end{bmatrix} \\
&= \begin{bmatrix}
\frac{\kappa_i s_i^2\cos(\phi_i)(\kappa_i^2 s_i^2-12))}{24} \\
\frac{(\kappa_i s_i^2\sin(\phi_i)(\kappa_i^2 s_i^2-12))}{24} \\
\frac{s_i-(\kappa_i^2 s_i^3)}{6}
\end{bmatrix}, \quad \text{for } i=1,2
\end{aligned} \tag{2}
$$

B. DIFFERENTIAL KINEMATICS

In the following, the section index i is omitted for simplicity, while being implicitly included unless other is mentioned. The tip linear velocity $\boldsymbol{v} = \dot{\boldsymbol{p}} \in \boldsymbol{R}^3$ of the robot end-effector relative to the base frame is related to the time derivatives of the configuration space variables of two sections continuum robot, $\boldsymbol{q} = [s_i, \kappa_i, \phi_i, s_{i+1}, \kappa_{i+1}, \phi_{i+1}]^T \in \boldsymbol{R}^6$, where $i=1$ as follows,

$$\dot{\boldsymbol{p}} = J_p(\boldsymbol{q})\,\dot{\boldsymbol{q}} \tag{3}$$

where $J_p \in R^{3\times 6}$ is the Jacobian matrix which could be computed analytically as follows,

$$J_p = \frac{\partial(\boldsymbol{p})}{\partial(\boldsymbol{q})} = \frac{\partial(\boldsymbol{p})}{\partial(s_i, \kappa_i, \phi_i, s_{i+1}, \kappa_{i+1}, \phi_{i+1})}, \quad \text{for } i=1 \tag{4}$$

The angular velocity vector $\boldsymbol{\omega}$ of section i relative to its base coordinate can be also computed as follows [25],

$${}^{i-1}\boldsymbol{\omega}_i = {}^{i-1}\hat{\boldsymbol{t}}_i\,{}^{i-1}\dot{\boldsymbol{t}}_i, \quad \text{for } i=1,2 \tag{5}$$

where ${}^{i-1}\hat{\boldsymbol{t}}_i$ and ${}^{i-1}\dot{\boldsymbol{t}}_i$ are skew symmetric matrix and derivative of the tangent vector respectively which represents the last column vector of the rotation matrix ${}^{i-1}R_i$ [25].

The robot tip position relative to the base frame is computed as:

$${}^0\boldsymbol{p}_2 = {}^0\boldsymbol{p}_1 + {}^0R_1\,{}^1\boldsymbol{p}_2 \tag{6}$$

where ${}^0\boldsymbol{p}_1$ and ${}^1\boldsymbol{p}_2$ is the position of endpoint of each section relative to its base which obtained from (2) and ${}^0R_1$ represents the rotation matrix of the first section relative to the base frame that can be easily computed from (1) for $i=1$.

The linear velocity of the end-effector relative to the base frame can also be derived by direct differentiation of (6) with respect to time as follows:

$${}^0\boldsymbol{v}_2 = {}^0\dot{\boldsymbol{p}}_1 + {}^0\dot{R}_1\,{}^1\boldsymbol{p}_2 + {}^0R_1\,{}^1\dot{\boldsymbol{p}}_2 \tag{7}$$

Also, the angular velocity of the end-effector relative to the base frame can be calculated as follows:

$$^{0}\boldsymbol{\omega}_2 = {}^{0}\boldsymbol{\omega}_1 + {}^{0}R_1\,{}^{1}\boldsymbol{\omega}_2 \tag{8}$$

III. DYNAMIC MODELING

Despite the extensive research on kinematic modeling of continuum robots, far too little attention has been paid to derive their complete dynamic model that could be challenging due to the increased Degree of Freedom (DOF) of continuum robots, especially in spatial environments. For instance, in [26], [27], a three-dimensional dynamic model of a non-extensible flexible manipulator was developed based on Newton-Euler, Lagrange and regressor representations. The flexible robot was considered as a set of stacked slices where each slice was considered as a rigid link with an infinitesimal width. The planar dynamics of a three-section extensible continuum robot was obtained in [28], [29] without considering the robot torsional effect. In [30], the dynamic modeling of a pneumatic-driven continuum robot based on the constant curvature kinematics and the Euler-Lagrange formalism was developed. The developed model neglected the rotational energies resulting from angular velocities that could affect the overall equations of motion. The dynamic model of planer continuum manipulator was proposed in [31], considering its backbone as two circular arcs. The obtained model was tested using practical thick NiTinol rod which used as a continuous backbone. The results showed that the error between the simulation and experimental tip trajectories was significant. In [25], the dynamic modeling of a planar two-section continuum robot was derived based on the Taylor Expansion method to overcome the singularities appeared in the robot's kinematic model. A PID control algorithm with trial and error selected gains was used for tracking the robot's tip trajectory. However, the results showed that the developed dynamic model can not be used for extensible type robots.

In this section, the dynamic model of extensible two-section continuum robot is introduced. The mass of each section, which is assumed to be flexible solid cylinder, is distributed along the section length, while the center of mass of each section m_i is assumed to be concentrated at the end of each section as shown in Fig. 2. Each bending section i is modeled as spring-damper model in the longitudinal direction as well as in the bending direction about the center of curvature. Namely, H_{s_i} and D_{s_i} are spring stiffness and the damping in the longitudinal direction, while H_{t_i} and D_{k_i} are those in the bending direction about the center of curvature.

To derive the dynamic equations of n sections continuum robot, the Lagrange equations along the generalized coordinates $\boldsymbol{q} \in \mathbb{R}^6$ is given by

$$\frac{d}{dt}\frac{\partial L}{\partial \dot{q}} - \frac{\partial L}{\partial q} + \boldsymbol{f}_\delta = \boldsymbol{\tau} \tag{9}$$

where $L = K - P$ is the Lagrangian that denotes the difference between the kinetic energy K and the potential energy P, while $\boldsymbol{\tau}$ represents the generalized forces acting on the generalized robot coordinates and $\boldsymbol{f}_\delta$ represents the dissipative forces which is the forces generated due to longitudinal damping $[D_{s_1}, D_{s_2}]$ and torsional damping $[D_{\kappa_1}, D_{\kappa_2}]$ respectively that can be computes as follows:

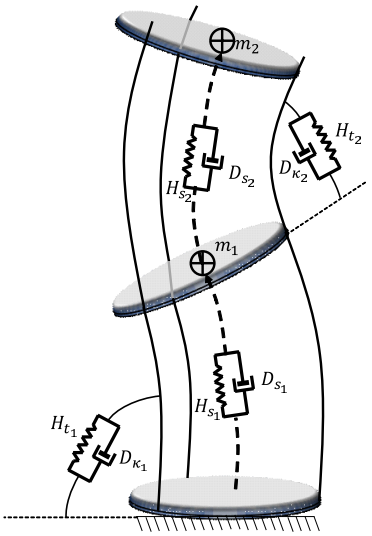

FIGURE 2. Two-section continuum robot modeled as a spring-damper system acting on its length.

$$\boldsymbol{f}_\delta = \frac{1}{2}\begin{bmatrix} D_{s_1}\dot{s}_1^2 \\ D_{\kappa_1}\dot{\kappa}_1^2 \\ 0 \\ D_{s_2}\dot{s}_2^2 \\ D_{\kappa_2}\dot{\kappa}_2^2 \\ 0 \end{bmatrix} \tag{10}$$

In this paper, the values of damping coefficients $[D_{s_1}, D_{s_2}, D_{\kappa_1}, D_{\kappa_2}]$ are assumed values.

A. KINETIC ENERGY

The total kinetic energy is the sum of translational and rotational energies of the end point of each bending section which can be calculated as follows:

$$K = \sum_{i=1}^{2} K_{t_i} + K_{r_i} \tag{11}$$

where K_{t_i} represents the translational energy which is computed as follows:

$$K_{t_i} = \frac{1}{2}{}^{0}\boldsymbol{v}_i^{\,T}\, m_i\, {}^{0}\boldsymbol{v}_i \tag{12}$$

where m_i is the mass of each bending section and ${}^{0}\boldsymbol{v}_i$ represents the velocity of the center of mass of each bending section relative to the base frame. By applying the first time derivative of (2) for $i = 1$, the velocity of the center of mass of the first bending section relative to the base frame can be computed while that of the second bending section relative to the base frame is obtained from (7).

Also, the rotational energy K_{r_i} is obtained as follows:

$$K_{r_i} = \frac{1}{2}{}^{0}\boldsymbol{\omega}_i^{\,T}\, I_i\, {}^{0}\boldsymbol{\omega}_i \tag{13}$$

where I_i is the inertia tensor matrix of each bending section.

B. POTENTIAL ENERGY

The potential energy P is obtained as follows,

$$P = P_g + P_e \tag{14}$$

where P_g and P_e represents the gravitational part and the elastic part respectively which are computed as follows:

$$P_g = \sum_{i=1}^{2} \boldsymbol{g}^T \boldsymbol{p}_i m_i \tag{15}$$

$$P_e = \frac{1}{2} \sum_{i=1}^{2} H_{s_i} \left(s_i - s_{i_0}\right)^2 + H_{t_i} s_i^2 (\kappa_i - \kappa_{i_0})^2 \tag{16}$$

where $\boldsymbol{p}_i = [x_i\ y_i\ z_i]^T$ is the robot's tip position vector, $\boldsymbol{g} \in \mathbb{R}^3$ is the gravitational acceleration vector, s_{i_0} represents the initial arc length, while κ_{i_0} is the initial curvature. H_{s_i} is the stiffness [32] and H_{t_i} is torsional spring constant [25] which can be obtained as follows:

$$\begin{aligned} H_{s_i} &= \frac{EA_i}{s_i} \\ H_{t_i} &= \frac{EI_{b_i}}{2s_i} \quad \text{for } i = 1, 2 \end{aligned} \tag{17}$$

where E is the modulus of elasticity, A_i is the cross sectional area of each section and I_{b_i} represents the second moment of cross-sectional area of each section. However in this paper, the values of H_{s_i} and H_{t_i} are assumed values.

C. GENERALIZED FORCES

The generalized forces $\boldsymbol{\tau}$ in (9) are the actuation forces acting on the robot to change the robot length and configuration. These forces are resulting from tension forces for the two sections $\boldsymbol{\tau} = [\tau_1, \tau_2, \tau_3, \tau_4, \tau_5, \tau_6]^T \in \mathbb{R}^6$ which are applied by six servo motors to change the robot section lengths s_i, curvatures κ_i and angles of curvature ϕ_i for $i = 1, 2$.

D. RESULTING DYNAMIC MODEL

By computing the Lagrangian L, it's derivatives and the generalized forces, the the equation of motion in (9) can be represented in a matrix form as follows:

$$M(\boldsymbol{q})\ddot{\boldsymbol{q}} + C(\boldsymbol{q}, \dot{\boldsymbol{q}})\dot{\boldsymbol{q}} + \boldsymbol{G}(\boldsymbol{q}) + \boldsymbol{f}_\delta = \boldsymbol{\tau} \tag{18}$$

where $M(\boldsymbol{q}) \in \mathbb{R}^{6\times6}$ is the inertia matrix, $C(\boldsymbol{q}, \dot{\boldsymbol{q}}) \in \mathbb{R}^{6\times6}$ is the Coriolis and Centrifugal matrix and $\boldsymbol{G}(\boldsymbol{q}) \in \mathbb{R}^{6\times1}$ represents the gravitational vector.

IV. DEMONSTRATION-BASED POSE PLANNING

A. COLLECTION OF DEMONSTRATIONS

A flexible input interface consists of two flexible rods stacked over each other to resemble precisely the kinematics of two-section continuum robot. The flexible interface is made of NINJA FLEX soft rubber material which is printed using 3D printer machine. Two 6050-MPUs IMU sensors are mounted on the end of each flexible rod to collect the orientation trajectories of the interface in unit quaternion form during motion as shown in Fig. 3. It is worth to note that the collected

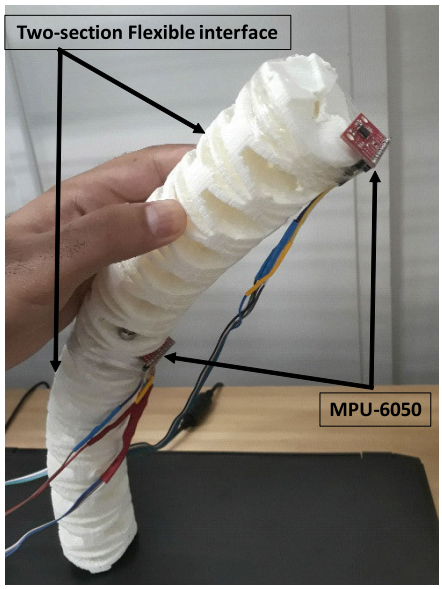

FIGURE 3. Two-section flexible interface.

sensors data are measured relative to the base frame. Based on the rotation matrix of the robot which is computed from (1) and the orientation of the interface obtained from MPUs sensors, the robot geometric parameters of each section κ_i and ϕ_i are presented as in [22].

$$\begin{aligned} \kappa_i &= \frac{\cos^{-1}\left(1 - 2(Q_{xi}^2 + Q_{yi}^2)\right)}{s_i}, \quad \kappa_i > 0 \\ \phi_i &= \tan^{-1}\left(\frac{Q_{xi}Q_{wi} + Q_{yi}Q_{zi}}{q_{xi}Q_{zi} - Q_{yi}Q_{wi}}\right), \quad -\pi \le \phi_i \le \pi \end{aligned} \tag{19}$$

where $i = 1, 2$, Q_w and $[Q_x, Q_y, Q_z]^T$ are the scalar and the vector components of the measured orientation input $\boldsymbol{Q}$. Based on the computed values of κ_i and ϕ_i in (19) with each section length s_i for $i = 1, 2$, the positions of the end-effector of the first and second sections of the flexible interface relative to the base frame can be computed easily from the last column of (1).

B. DYNAMIC MOVEMENT PRIMITIVES

The Dynamic Movement Primitives (DMP) is an efficient way for learning and control of complex demonstrated discrete or rhythmic robot behaviors [33]. In this paper, the point-to-point discrete movement is considered for multi-section continuum robots.

1) POSITION BASED-DMP

A DMP for each DOF of the demonstrated motion is represented by the following set of differential equations [34],

$$\lambda \dot{v}_t = \beta\left(\gamma(g_p - x_t) - v_t\right) + \left(g_p - x_0\right) f(s_d) \tag{20}$$

$$\tau \dot{x}_t = v_t \tag{21}$$

where x_t and v_t are the position and velocity of each DOF in the system, g_p represents the goal position, x_0 is the

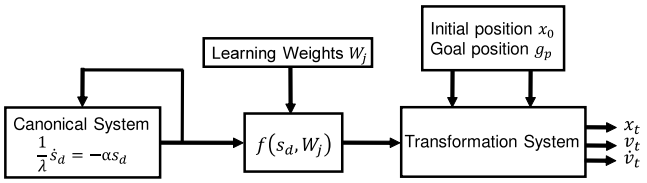

FIGURE 4. A one-dimensional DMP schematic diagram.

initial position, while λ, β, and γ are tuning parameters. Three DMPs are incorporated for position coordinates in this section. The forcing term $f(s_d)$ in (20) is a linear function composed of N nonlinear radial basis functions, which are learned from the given demonstrations to allow the robot to follow any arbitrary complex motions from initial position x_0 to the goal position g_p as follows,

$$f(s_d) = \frac{\sum_{j=1}^{N} W_j \psi_j(s_d) s_d}{\sum_j \psi_j(s_d)} \tag{22}$$

In which

$$\psi_j(s_d) = \exp(-h_j(s_d - c_j)^2) \tag{23}$$

where c_j and h_j are the centers and width of radial basis function respectively and W_j represents the adjustable weights. The phase variable s_d is used to avoid the explicit dependence on time. This variable is monotonically decaying from 1 to 0 during the movement which is computed by integrating the following first order linear dynamic equation,

$$\frac{1}{\lambda}\dot{s}_d = -\alpha s_d \tag{24}$$

where α is a pre-defined positive constant.

The DMP is a spatial and temporal invariant; namely, it is an adaptive learning technique to either any changes in the initial and goal positions or the time scale with no need to re-learn the weights W_j again. As shown in Fig. 4, to learn movement from demonstration, the demonstrated position x_t, velocity v_t and acceleration $\dot{v}_t$ are computed at each time step $t = 0, 1, 2, \ldots, T$. Then, $s_d(t)$ is computed by integrating the canonical system for a certain temporal scaling λ from equation (24). Using these variables, the target force $f_{target}(s_d)$ is computed based on (20) as follows,

$$f_{target}(s_d) = \frac{\lambda \dot{v}_t - \beta\left(\gamma(g_p - x_t) - v_t\right)}{\left(g_p - x_0\right)} \tag{25}$$

Learning is done by obtaining the set of weights W_j which minimizes the sum of square error $\sum_{s_d}\left(f_{target}(s_d) - f(s_d)\right)^2$ between the generated force from (22) and the target force in (25). By reusing the learned weights W_j, the observed motion is generated by obtaining the corresponding acceleration in (20). The velocity and position are obtained by the first and the second time integration of (20).

a: GENERALIZATION TO NEW GOALS

New unobserved movements could be created for the continuum robot from the learned DMP equations. In this regard, by keeping on the so far learned weights W_j, new motions could be obtained in terms of x_t, v_t and $\dot{v}_t$ for each DOF by changing either the spatial, (x_0 or g), or the temporal λ scales in (20).

b: OBSTACLE AVOIDANCE

To avoid static or dynamic obstacles that could exist on the DMP generated path, a coupling term $\boldsymbol{p}(\boldsymbol{x}, \boldsymbol{v})$ is added to the differential equation in (20) [35],

$$\lambda \dot{\boldsymbol{v}} = \beta\left(\gamma(\boldsymbol{g} - \boldsymbol{x}) - \boldsymbol{v}\right) + \boldsymbol{f}(s_d) + \boldsymbol{p}(\boldsymbol{x}, \boldsymbol{v}) \tag{26}$$

The obstacle avoidance form is described in 3D end-effector space, therefore, the parameters $\boldsymbol{g}, \boldsymbol{x}, \boldsymbol{v}, \dot{\boldsymbol{v}}$ and $\boldsymbol{f}$ are expressed in vector form for the combined three DOF of the robot tip position. The coupling term $\boldsymbol{p}(\boldsymbol{x}, \boldsymbol{v})$ can be implemented for the obstacle avoidance dynamics which is described as follows [11],

$$\boldsymbol{p}(\boldsymbol{x}, \boldsymbol{v}) = \eta_1 R \boldsymbol{v} \varphi \exp(-\eta_2 \varphi) \tag{27}$$

where η_1 and η_2 are constants that can be selected based on the obstacle size and φ is the angle between the position of the tip of the robot $\boldsymbol{x}$ towards the position of the obstacle $\boldsymbol{o}$ and the robot tip velocity $\boldsymbol{v}$. The rotation matrix $R(\boldsymbol{r}, \pi/2)$ is chosen with an axis of rotation $\boldsymbol{r} = (\boldsymbol{x} - \boldsymbol{o}) \times \boldsymbol{v}$ and with a $\pi/2$ angle.

2) ROTATION BASED DMP

Describing the robot's end-effector pose in the Cartesian space needs specifying the position trajectories, as well as orientation trajectory $R(t) \in \mathbb{R}^{3\times3}$. The coefficients of the rotation matrix $R(t)$ could be represented by the DMP system similar to (20)-(21). However, the coefficients of the orientation trajectory $R(t)$ are dependent on each other. Therefore, by integrating them independently, the obtained rotation trajectory will gradually deviate from the actual one. By reformulating (20)-(21) as presented in [34], the DMP system for representing orientation trajectory is as follow:

$$\lambda \dot{\boldsymbol{\eta}} = \beta\left(\gamma \log(R_g R^T) - \boldsymbol{\eta}\right) + \boldsymbol{f_r}(s_d) \tag{28}$$

$$\lambda \dot{R} = [\eta]_\times R \tag{29}$$

where R_g represents the goal orientation matrix, $\boldsymbol{\eta}$ is the scaled angular velocity of $\boldsymbol{\omega}$ which means $\boldsymbol{\eta} = \lambda\boldsymbol{\omega}$, $\dot{\eta} = \tau\dot{\omega}$, $[\eta]_\times$ is the skew matrix of $\boldsymbol{\eta}$ which obtained as $[\eta]_\times = \tau\,[\omega]_\times$ and $f_r(s_d)$ is the nonlinear forcing term which is computed as follows:

$$f_r(s_d) = G_r \frac{\sum_{j=1}^{N} w_j^r \psi_j(s_d) s_d}{\sum_j \psi_j(s_d)} s_d \tag{30}$$

where $G_r = diag(\log(R_g R^T)) \in \mathbb{R}^{3\times3}$ is a scaling factor matrix and $w_j^r \in \mathbb{R}^3$ are adjustable weights which need to be computed for following any generated orientation trajectory. The term w_j^r is computed by using linear least square regression technique of the following equation:

$$\frac{\sum_{j=1}^{N} w_j^r \psi_j(s_d) s_d}{\sum_j \psi_j(s_d)} s_d = G_r^{-1}\left(\tau\dot{\eta}_c + \beta\eta_c - \beta\gamma \log(R_g R_c^T)\right) \tag{31}$$

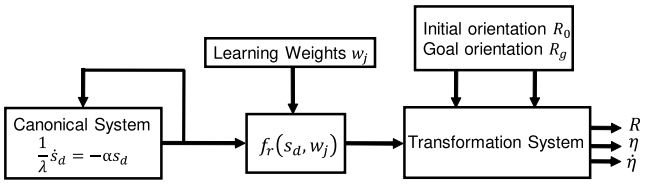

FIGURE 5. Schematic diagram of rotation based DMP.

where R_c, η_c and $\dot{\eta}_c$ are the collected rotation matrix, scaled angular velocity and scaled angular acceleration vectors respectively. The schematic diagram of rotation based DMP is shown in Fig. 5.

The rotation matrix is obtained by integrating technique of (29) as follows:

$$R(t + \Delta t) = \exp(\Delta t \left(\frac{[\eta]_x}{\lambda}\right) R(t) \tag{32}$$

V. CONTROL ALGORITHM

A. MODEL REFERENCE ADAPTIVE KINEMATIC CONTROL

The model reference adaptive kinematic control (MRAKC) is developed here to solve the inverse kinematics of the continuum robot. The generated motion from DMP approach is expressed as a set of position, velocity and acceleration vectors which the robot end-effector needs to follow to reach the desired goal. Due to redundant DOF of the continuum robot, it's a challenging problem to transform the joint space trajectory to the configuration space variables (s, κ, ϕ) of the robot. So, a Jacobian- based kinematic control is used to find incrementally the robot's configuration parameters to make the continuum robot track the obtained reference trajectories by the DMP.

Regarding the robot orientation, unit quaternion is used for representing the continuum robot rotation. Rather than representing the robot rotation by the traditional methods such as Euler angels, Axis-angle and rotation matrices, representing this rotation using unit quaternion provides a lot of advantageous such as singularity free, efficient and compactness [36].

The relations between unit quaternion vector $Q = \left[Q_w \; Q_x \; Q_y \; Q_z\right]^T$ and rotation matrix in (1) can be written as [37]:

$$\begin{bmatrix} Q_w \\ Q_x \\ Q_y \\ Q_z \end{bmatrix} = \begin{bmatrix} \frac{\sqrt{R_{11} + R_{22} + R_{33} + 1}}{2} \\ \frac{R_{32} - R_{23}}{4A} \\ \frac{R_{13} - R_{31}}{4A} \\ \frac{R_{21} - R_{12}}{4A} \end{bmatrix} \tag{33}$$

where R_{ij} is ij^{th} the element of the rotation matrix.

The MRAKC scheme is developed here with the following key steps as follows,

a: JACOBIAN-BASED CONTROLLER

The robot's configuration parameters are related to robot tip velocity $\dot{\boldsymbol{Z}} = \left[\dot{\boldsymbol{p}} \; \dot{\boldsymbol{Q}}\right]^T$, where $\dot{\boldsymbol{p}}$ and $\dot{\boldsymbol{Q}}$ represent the linear velocities vector and the rotation angles velocities vector respectively, as follows:

$$\dot{\boldsymbol{q}} = \mathbf{J}^{\dagger}(\boldsymbol{q})\, \dot{\boldsymbol{Z}} \tag{34}$$

where $J^{\dagger} \in \mathbb{R}^{6\times7}$ represent the pseudo inverse of the Jacobian matrix $J \in \mathbb{R}^{7\times6}$ that is not a square matrix and can be computed as follows:

$$J = \frac{\partial(\boldsymbol{Z})}{\partial(\boldsymbol{q})} = \frac{\partial(\boldsymbol{Z})}{\partial(s_i, \kappa_i, \phi_i, s_{i+1}, \kappa_{i+1}, \phi_{i+1})} \quad \text{for } i = 1 \tag{35}$$

To eliminate the numerical drift while following the desired trajectory, a feedback correction term is introduced here [38]. Then, the configuration velocities vector is introduced as follows,

$$\dot{\boldsymbol{q}} = \mathbf{J}^{\dagger}(\dot{\boldsymbol{Z}}_d + K\boldsymbol{e}_k) \tag{36}$$

where $\boldsymbol{e}_k = \boldsymbol{Z}_d - \boldsymbol{Z}$ is the error between the reference and the actual tip position and rotation angles vectors, while $K \in R^{7\times7}$ is a positive definite gain matrix, which is selected to be diagonal for stability analysis purpose. The configuration parameters of two sections robot $s_i, \kappa_i, \phi_i, s_{i+1}, \kappa_{i+1}$ and ϕ_{i+1} for $i = 1$, are determined by integrating (36) with respect to time.

b: ADAPTATION MECHANISM

Due to the external disturbances and the model uncertainties that could exist, the gains K in equations (36) respectively have to be adapted as follows,

$$K = \int_0^t \gamma_a \left|\boldsymbol{e}_a^T \bar{\boldsymbol{Z}}\right| dt \tag{37}$$

where $|.|$ represents the absolute value, γ_a determines the rate of adaptation, $\boldsymbol{e}_a = \boldsymbol{Z} - \bar{\boldsymbol{Z}}$ denotes the difference between the reference model output $\bar{\boldsymbol{Z}}$ and the actual behaviors of the system as depicted in Fig. 6. It is worth to note that the reference behavior is arbitrary selected based on the desired performance in terms of overshoot, settling time. In this paper, the reference model is chosen as a second order transfer function.

B. DYNAMIC CONTROL

The computed torque controller is a feedback linearization technique of nonlinear systems in which the original nonlinear system is transferred into a fully or partly linear system by inserting the system nonlinearities into the control signal [39].

From dynamic model (18), the acceleration is computed as follows

$$\ddot{\boldsymbol{q}} = M(\boldsymbol{q})^{-1}\left(\boldsymbol{\tau} - C(\boldsymbol{q}, \dot{\boldsymbol{q}})\dot{\boldsymbol{q}} - G(\boldsymbol{q}) - \boldsymbol{f}_{\delta}\right) \tag{38}$$

The actuation force $\boldsymbol{\tau}$ is obtained from the following equation [40]:

$$\boldsymbol{\tau} = M(\boldsymbol{q})\left(\ddot{\boldsymbol{q}}_d - u\right) + C(\boldsymbol{q}, \dot{\boldsymbol{q}})\dot{\boldsymbol{q}} + \boldsymbol{G}(\boldsymbol{q}) + \boldsymbol{f}_{\delta} \tag{39}$$

where the control signal u is chosen as proportional-derivative (PD) feedback as follows:

$$\boldsymbol{u} = -K_p\boldsymbol{e} - K_v\dot{\boldsymbol{e}} \tag{40}$$

where $\dot{\boldsymbol{e}} \in \mathbb{R}^{6\times1}$ is the error vector between the reference and actual configuration parameters of the robot, $K_p \in \mathbb{R}^{6\times6}$ and $K_v \in \mathbb{R}^{6\times6}$ represent the proportional and derivative gains matrices which are chosen positive gain matrices for ensuring the system stability [40]. The schematic of PD computed torque dynamic control with adaptive kinematic control is shown in Fig. 6.

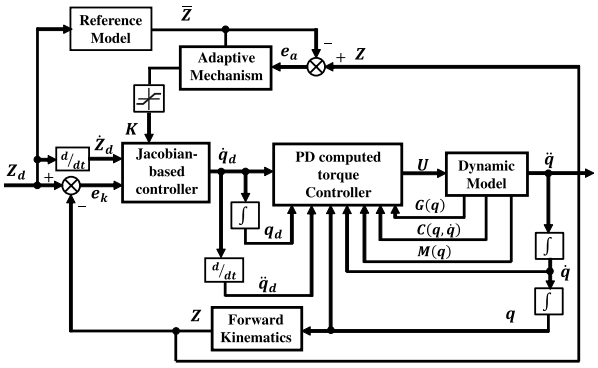

FIGURE 6. Dynamic with adaptive kinematic control for the robot tip position tracking.

VI. STABILITY ANALYSIS

Starting with the stability analysis of the kinematic control, the Lyapunov function is chosen as a quadratic function [41] as follows:

$$V(\boldsymbol{e}_k) = \frac{1}{2}\boldsymbol{e}_k^T\boldsymbol{e}_k \tag{41}$$

For ensuring that the system is global asymptotically stable, the first time derivative of $V(\boldsymbol{e}_k)$ must be negative definite and the error $\boldsymbol{e}_k$ exponentially decreases to zero [39]. The time derivative of $V(\boldsymbol{e}_k)$ can be written as:

$$\dot{V}(\boldsymbol{e}_k) = \boldsymbol{e}_k^T\dot{\boldsymbol{e}}_k \tag{42}$$

where $\dot{\boldsymbol{e}}_k = \dot{\boldsymbol{Z}}_d - \dot{\boldsymbol{Z}}$.

By substituting the values of $\dot{\boldsymbol{Z}}_d$ from (36) and $\dot{\boldsymbol{Z}}$ from (34) in (42), the following can be obtained:

$$\begin{aligned}\dot{V}(\boldsymbol{e}_k) &= \boldsymbol{e}_k^T\left[(J\dot{\boldsymbol{q}} - K\boldsymbol{e}_k) - J\dot{\boldsymbol{q}}\right]\\ &= -\boldsymbol{e}_k^T K\boldsymbol{e}_k\end{aligned} \tag{43}$$

According to (43), the diagonal gain matrix K must be positive definite diagonal matrix to make the system global asymptotically stable while applying the kinematic control.

Regrading applying the PD computed torque dynamic control, the Lyapunov function is considered as follows [42]:

$$V(\boldsymbol{e},\dot{\boldsymbol{e}}) = \frac{1}{2}\dot{\boldsymbol{e}}^T\dot{\boldsymbol{e}} + \frac{1}{2}\boldsymbol{e}^T K_p\boldsymbol{e} \tag{44}$$

where the first and the second terms represent the kinetic energy and potential energy of the robot induced by the first time derivative of the error and the error of the controller equation (39).

Differentiating of $V(\boldsymbol{e},\dot{\boldsymbol{e}})$ with respect to time yields:

$$\dot{V}(\boldsymbol{e},\dot{\boldsymbol{e}}) = \dot{\boldsymbol{e}}^T\ddot{\boldsymbol{e}} + \boldsymbol{e}^T K_p\dot{\boldsymbol{e}} \tag{45}$$

By substituting the control signal (39) in the dynamic model (18), the closed loop system equation is as follows:

$$\begin{aligned}M\left(\ddot{\boldsymbol{q}}_d - \ddot{\boldsymbol{q}}\right) + MK_v\dot{\boldsymbol{e}} + MK_b\boldsymbol{e} &= 0\\ M\left(\ddot{\boldsymbol{e}} + K_v\dot{\boldsymbol{e}} + K_p\boldsymbol{e}\right) &= 0\end{aligned} \tag{46}$$

Since the inertia matrix M is positive definite matrix, so M^{-1} exists and it is bounded, thus the closed loop system equation (46) can be written as:

$$\ddot{\boldsymbol{e}} + K_v\dot{\boldsymbol{e}} + K_p\boldsymbol{e} = 0 \tag{47}$$

By multiplying the both sides of (47) by $\dot{\boldsymbol{e}}^T$, and then substituting the resulting equation into (45) yields:

$$\dot{V}(\boldsymbol{e},\dot{\boldsymbol{e}}) = -\dot{\boldsymbol{e}}^T K_v\dot{\boldsymbol{e}} \tag{48}$$

Since K_v is chosen as a positive diagonal matrix, then $\dot{V}(\boldsymbol{e},\dot{\boldsymbol{e}})$ becomes negative semi-definite matrix and the closed loop system is asymptotically stable.

VII. RESULTS AND DISCUSSION

The considered parameters of the proposed DGPP approach for teaching a two-section continuum robot how to plan it's motion are listed in Table 1. Via teleoperation, a flexible interface consists of 20 cm two rods stacked over each other is used to demonstrate the motion of the simulated two-section continuum robot. Six point-to-point demonstrations are carried out. In each demonstration, the teacher is asked to move the tip of the flexible rod from unknown pose to another, while detecting the corresponding motion of the simulated robot.

TABLE 1. Chosen values for the DGPP parameters and system dynamics.

Parameter	Description	Value
β	DMP parameter	14
γ	DMP parameter	3.5
k	No. of basis functions	50
α	Canonical system constant	15
η_1	Obstacle avoidance constant	1000
η_2	Obstacle avoidance constant	8
γ_p	MRAC position adaptation rate	0.01
γ_r	MRAC orientation adaptation rate	0.1
T_s	Sampling time	0.05 s
n	No. of guidance disks	6
d	Robot core to cable distance	2 cm
l_i	Robot cables range	[10, 18] cm
m_i	Robot cables mass	100 gm
$[D_{s_1}, D_{s_2}]$	Linear damping	[0.005, 0.005]
$[D_{\kappa_1}, D_{\kappa_2}]$	Torsional damping	[0.001, 0.001]
s_{i0}	Initial arc length	[10, 10]
κ_{i0}	Initial curvature	[0.01, 0.01]
H_{s_i}	Stiffness constant	[7, 7]
H_{t_i}	Torsional spring constant	[0.5, 0.5]
K_{pos}	Gain matrix for kinematic position control	[100,100,50]
K_{rot}	Gain matrix for kinematic orientation control	[200,200,100]

For instance, the robot tip trajectories in Cartesian space are fed to DGPP to reproduce and generalize the observed motions. The proposed DGPP successfully reproduced the robot tip position trajectories, as shown in Fig. 7, compared with the given demonstration with initial position $\boldsymbol{x}_0 = [-5.0729, 9.5311, 15.3555]^T$ cm and goal position $\boldsymbol{g}_0 = [11.8447, -0.6337, 14.0723]^T$ cm. The motion simulation of

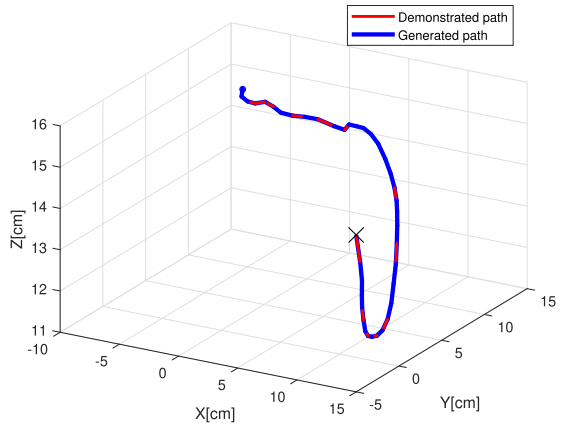

FIGURE 7. Reproduction of the observed motion through the proposed DGPP. Th optimized gains $[\beta, \gamma, \alpha] = [40.89, 18.86, 5.487]$.

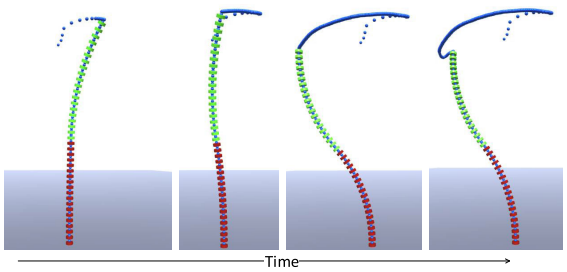

FIGURE 8. Snapshots of the generated motion.

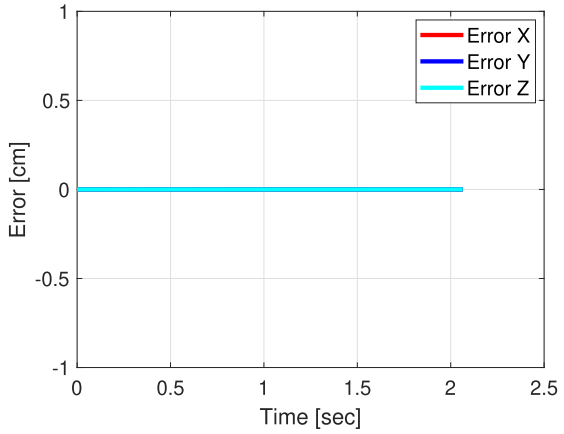

FIGURE 9. Error between the learned and demonstrated robot tip positions.

the robot tip is shown in Fig. 8. The errors between the learned and demonstrated motions are shown in Fig. 9.

Moreover, the generalization capability has been evaluated using the proposed DGPP by changing the initial and goal positions of the robot tip, while keeping on the learned weights, as shown in Fig. 10 and Fig. 11, respectively. The generated motion has successfully adapted to the new initial and goal positions while keeping on the learned point-to-point pattern. This operation could be useful in repetitive tasks applications with different initial or goal positions such as

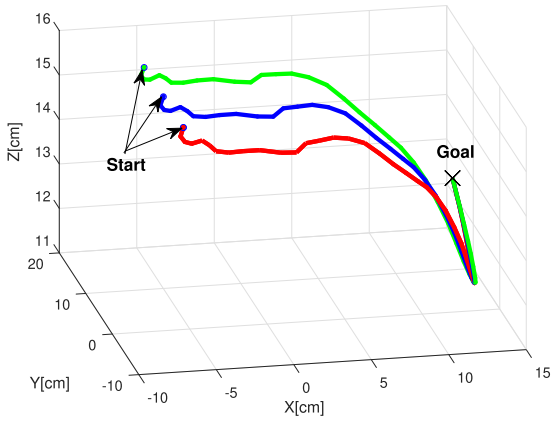

FIGURE 10. Adaptation of the learned motion to a set of new initial positions.

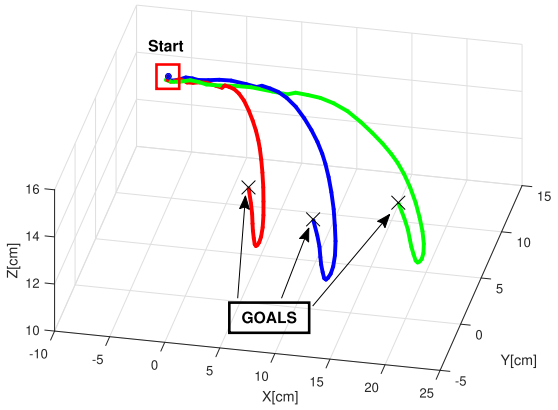

FIGURE 11. Adaptation of the learned motion to a set of new goals.

pick and place objects with no need to retrain the robot for each task individually.

Furthermore, the DGPP approach has successfully avoided a spherical shape obstacle which is placed in the same way of the robot tip path as shown in Fig. 12. The Cartesian position of obstacle is given to DGPP approach which could be obtained easily using range sensor or Kinect camera in real environment. In this phase of reproduction, the DGPP technique can balance between avoiding the fixed obstacle and moving towards the target. Also, DGPP can easily avoid a moving obstacle which is introduced along a segment of the given demonstration as shown in Fig. 13. The maximum velocity of the robot tip while avoiding the moving obstacle is 19.4702 cm/sec which is larger than the obstacle velocity 18.7742 cm/sec to reach successfully to the target position without any obstacle collision.

It is worth noting that, although the similarity between the demonstrated and the generated movements, there is no guarantee to shape the robot in the same way as the flexible interface shape during demonstrations. This, in fact, is due to the robot redundancy where infinite values of cable lengths can produce the same tip position in task-space. This encourages us to apply the proposed DGPP framework in

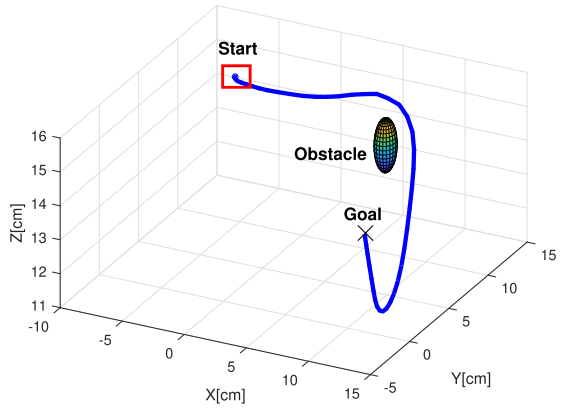

FIGURE 12. Adaptation of the demonstrated path to avoid novel obstacles in the environment. Th optimized gains $[\beta, \gamma, \alpha] = [20, 5, 6.9078]$.

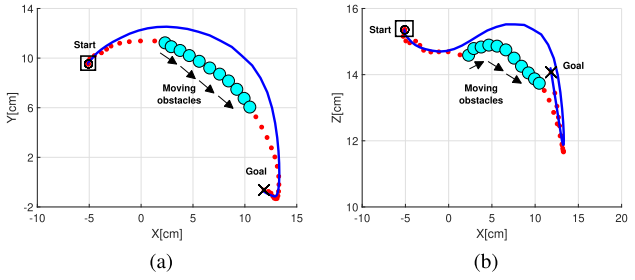

FIGURE 13. Adaptation of the demonstrated path to avoid moving obstacles. Th optimized gains $[\beta, \gamma, \alpha] = [15, 15, 6.9078]$.

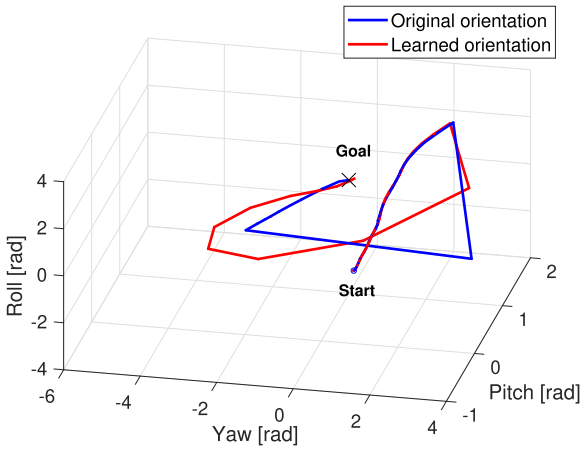

FIGURE 14. Reproduction of of the observed robot tip orientation trajectories.The optimized gains $[\beta, \gamma, \alpha] = [6.247, 4.703, 28.675]$.

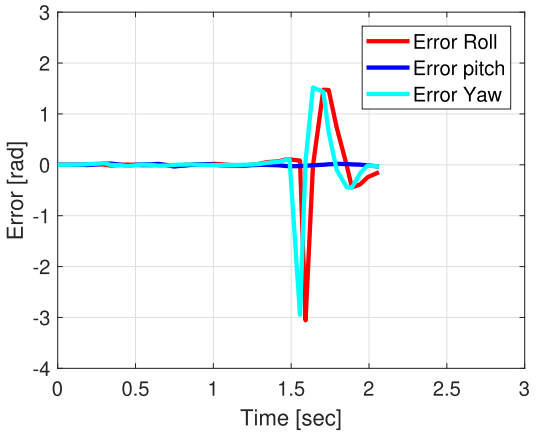

FIGURE 15. Error between the demonstrated and learned of the robot tip orientation trajectories.

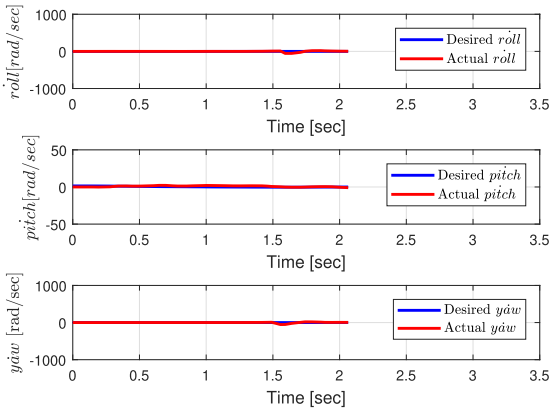

FIGURE 16. First time derivative of desired and actual roll, pitch and yaw angles.

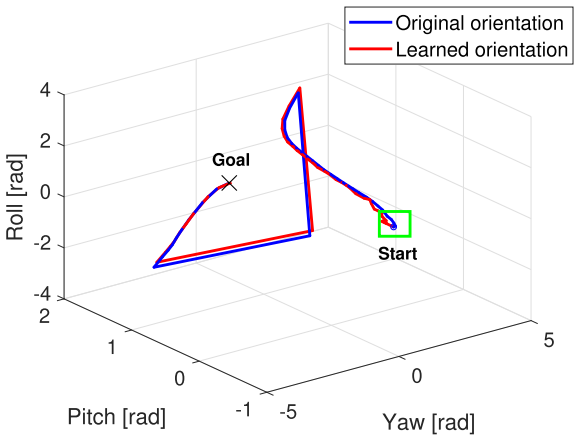

FIGURE 17. Adaptation of the demonstrated path to avoid novel obstacles in the environment.The optimized gains $[\beta, \gamma, \alpha] = [46.43, 49.24, 3.25]$.

the configuration or actuation spaces that could guarantee generating similar shapes. The rotation representation by roll, pitch and yaw angles using DMP based on (20)-(21) is shown in Fig. 14. The errors between the learned and demonstrated roll, pitch and yaw trajectories are shown in Fig. 15. Moreover, the first time derivative of desired and actual roll, pitch and yaw angles are shown in Fig. 16. It can be noted that, it is difficult to reproduce or generalize the end-effector orientation using the same method as that of the position. So, the orientation represented as roll, pitch and yaw trajectories based DMP is represented using (28)-(29) as illustrated in Fig. 17. The errors between the learned and demonstrated of roll, pitch and yaw trajectories are shown in Fig. 18. Also, the reference and actual time trajectories of the nine components of the rotation matrix are shown in Fig. 19. Finally, the first time

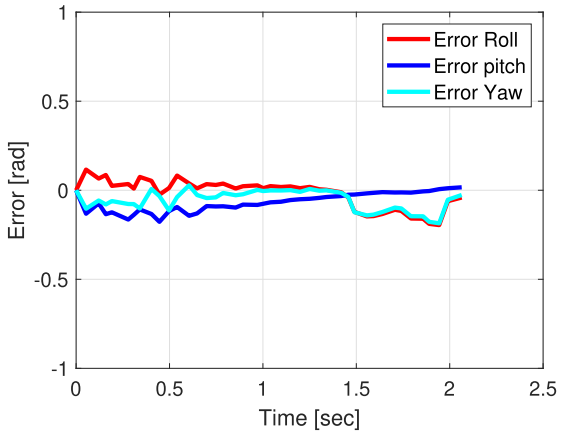

FIGURE 18. Error between the learned and demonstrated robot tip orientation trajectories.

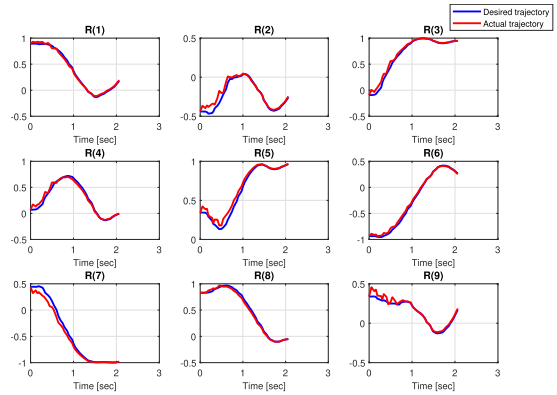

FIGURE 19. Desired and actual trajectories of nine components of rotation matrix.

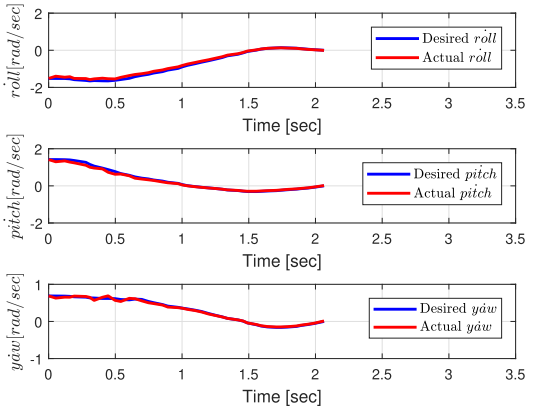

FIGURE 20. First time derivative of desired and actual roll, pitch and yaw angles.

derivative of desired and actual roll, pitch and yaw angles are shown in Fig. 20.

The performance of the developed MRAKC with PD computed torque control has been also evaluated towards tracking the robot tip position and orientation. The dynamics and control parameters are listed in Table 1.

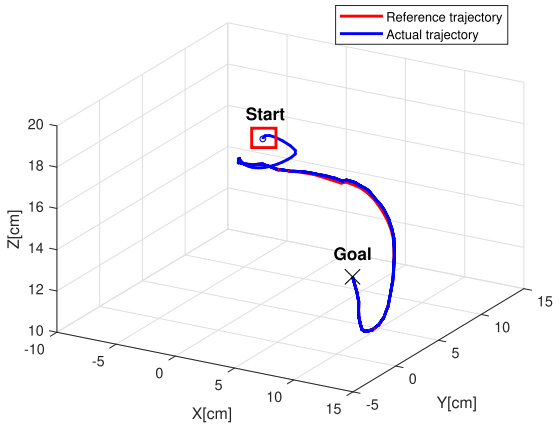

FIGURE 21. Reference and actual tip position trajectories.

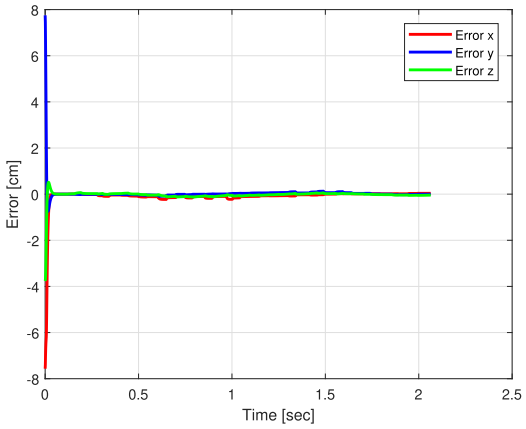

FIGURE 22. Error between reference and actual tip position trajectories.

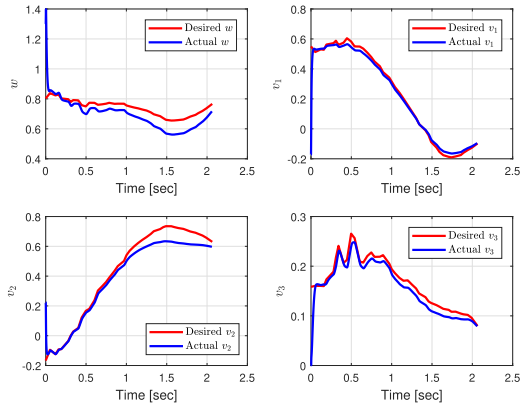

FIGURE 23. Reference and actual tip orientation trajectories.

First, regarding the robot tip position, the reference tip position trajectory versus the actual one are shown in Fig. 21. The tracking errors between the desired and actual tip position trajectories can be depicted in Fig. 22. Secondly, regarding the robot orientation, the desired and actual reference trajectories of the robot orientation represented by unit quaternion are shown in Fig. 23. The errors between the reference and actual orientation are shown in Fig. 24.

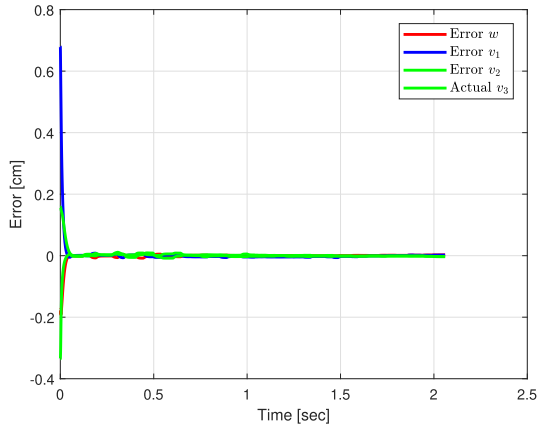

FIGURE 24. Error between reference and actual tip orientation trajectories.

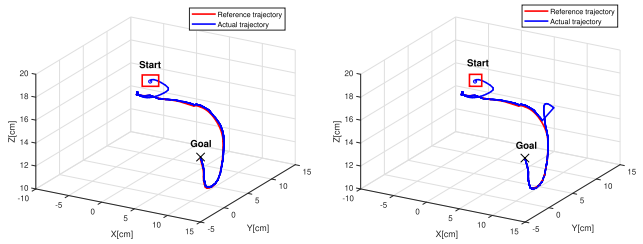

FIGURE 25. Reference and actual tip position trajectories after adding disturbance to (a) the controller signal. (b) the actual measured position.

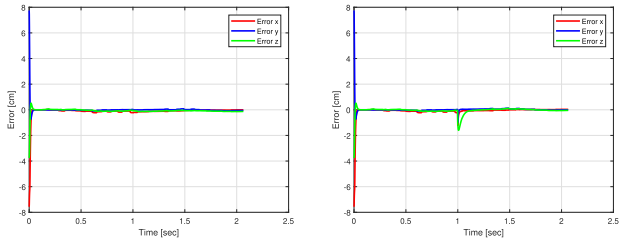

FIGURE 26. Tracking errors with disturbance to (a) the controller signal and to (b) the actual measured position.

As indicated, the actual trajectories follow precisely the reference trajectories except at the initial conditions of the robot since it is unknown to the controller. Meanwhile, the robustness of the proposed controller is evaluated by individually add a step disturbance to each of the control signal which is known as input disturbance and to the actual end-effector position of the robot. The reference and actual tip position trajectories after adding input and output disturbances are shown in Fig. 25(a) and Fig. 25(b) respectively. The error between the reference and actual tip trajectories after adding input and output disturbances are shown in Fig. 26(a) and Fig. 26(b) respectively.

VIII. CONCLUSION

In this research paper, a Demonstration Guided Pose Planning (DGPP) approach is developed to teach an extensible two-section continuum robot how to plan for it's point-to-point movements including position and orientation of the robot. The DGPP approach is used to reproduce the recorded movements with a set of nonlinear differential equations. Also, it can generate new motions with different initial and goal locations while avoiding fixed or movable obstacles which may exist in the environment. Via teleoperation, a two-rod flexible interface is used to intuitively demonstrate motions for the robot while the simulation of a two-section continuum robot is carried out to evaluate the feasibility of the proposed DGPP. Moreover, a complete dynamic model for extensible two-section continuum robot is developed based on Euler-Lagrange formalism with the Taylor expansion approach to avoid singularities. Finally, Model Reference Adaptive Kinematic Control (MRAKC) and Proportional-Derivative (PD) computed torque control are developed to ensure robustness of the kinematic and dynamic control of the robot against system perturbations and external disturbances that could exist. Moreover, the system stability analysis has been discussed based on Lyapunov quadratic function. The results have shown that the proposed DGPP approach is effective for reproducing the demonstrated position and orientation of the robot end-effector and also for generating movements with new initials, goals, fixed and moving obstacles. Also, results have shown superior performance towards generating spatial motions for the robot with a human-like adaptation to new goals, obstacles, and disturbances. As well as, the results have shown the performance of the adaptive kinematic and PD computed dynamic control against system uncertainties and disturbances.

In future work, the continuum robot tip position and orientation will be incorporated simultaneously in DMP based on dual-quaternion approach to improve the performance and speed of the motion planning approach. Furthermore, a practical validation of the proposed motion planning technique and the dynamic control will be carried on.

REFERENCES

[1] *World Robotics Report*, IFR Statistical Department, Frankfurt, Germany, 2017.
[2] D. Trivedi, C. D. Rahn, W. M. Kier, and I. D. Walker, "Soft robotics: Biological inspiration, state of the art, and future research," *Appl. Bionics Biomech.*, vol. 5, no. 3, pp. 99–117, 2008.
[3] P. H. Nguyen, C. Sparks, S. G. Nuthi, N. M. Vale, and P. Polygerinos, "Soft poly-limbs: Toward a new paradigm of mobile manipulation for daily living tasks," *Soft Robot.*, vol. 6, no. 1, pp. 38–53, 2018.
[4] C. S. Simpson, A. M. Okamura, and E. W. Hawkes, "Exomuscle: An inflatable device for shoulder abduction support," in *Proc. IEEE Int. Conf. Robot. Autom. (ICRA)*, May/Jun. 2017, pp. 6651–6657.
[5] J. Burgner-Kahrs, D. C. Rucker, and H. Choset, "Continuum robots for medical applications: A survey," *IEEE Trans. Robot.*, vol. 31, no. 6, pp. 1261–1280, Dec. 2015.
[6] K. Shahzad, S. Iqbal, and P. Bloodsworth, "Points-based safe path planning of continuum robots," *Int. J. Adv. Robotic Syst.*, vol. 12, no. 7, p. 107, 2015.
[7] A. H. Memar, M. Keshmiri, and K. Torabi, "Motion planning for a multi-segment continuum robot," in *Proc. Int. Conf. Mech. Eng. Mechatronics*, 2012, pp. 1–10.
[8] I. S. Godage, D. T. Branson, E. Guglielmino, and D. G. Caldwell, "Path planning for multisection continuum arms," in *Proc. Int. Conf. Mechatronics Autom. (ICMA)*, Aug. 2012, pp. 1208–1213.
[9] D. Hahnel, W. Burgard, D. Fox, and S. Thrun, "An efficient fastSLAM algorithm for generating maps of large-scale cyclic environments from raw laser range measurements," in *Proc. Int. Conf. Intell. Robots Syst. (IROS)*, vol. 1, Oct. 2003, pp. 206–211.

[10] O. Khatib, "Real-time obstacle avoidance for manipulators and mobile robots," in *Autonomous Robot Vehicles*. New York, NY, USA: Springer, 1986, pp. 396–404.
[11] P. Pastor, H. Hoffmann, T. Asfour, and S. Schaal, "Learning and generalization of motor skills by learning from demonstration," in *Proc. Int. Conf. Robot. Autom. (ICRA)*, May 2009, pp. 763–768.
[12] B. D. Argall, S. Chernova, M. Veloso, and B. Browning, "A survey of robot learning from demonstration," *Robot. Auto. Syst.*, vol. 57, no. 5, pp. 469–483, 2009.
[13] M. Hersch, F. Guenter, S. Calinon, and A. Billard, "Dynamical system modulation for robot learning via kinesthetic demonstrations," *IEEE Trans. Robot.*, vol. 24, no. 6, pp. 1463–1467, Dec. 2008.
[14] A. Pervez, A. Ali, J.-H. Ryu, and D. Lee, "Novel learning from demonstration approach for repetitive teleoperation tasks," in *Proc. World Haptics Conf. (WHC)*, Jun. 2017, pp. 60–65.
[15] S. Nakaoka, A. Nakazawa, K. Yokoi, H. Hirukawa, and K. Ikeuchi, "Generating whole body motions for a biped humanoid robot from captured human dances," in *Proc. Int. Conf. Robot. Autom. (ICRA)*, vol. 3, Sep. 2003, pp. 3905–3910.
[16] T. Kulvicius, K. Ning, M. Tamosiunaite, and F. Worgötter, "Joining movement sequences: Modified dynamic movement primitives for robotics applications exemplified on handwriting," *IEEE Trans. Robot.*, vol. 28, no. 1, pp. 145–157, Feb. 2012.
[17] D.-H. Park, H. Hoffmann, and S. Schaal, "Combining dynamic movement primitives and potential fields for online obstacle avoidance," in *Proc. 5th Int. Symp. Adapt. Motion Animals Mach.*, vol. 1. Cleveland, OH, USA: Case Western Reserve Univ., 2008, pp. 1–2.
[18] M. Kasper, G. Fricke, K. Steuernagel, and E. von Puttkamer, "A behavior-based mobile robot architecture for learning from demonstration," *Robot. Auto. Syst.*, vol. 34, nos. 2–3, pp. 153–164, 2001.
[19] H. Wang, J. Chen, H. Y. K. Lau, and H. Ren, "Motion planning based on learning from demonstration for multiple-segment flexible soft robots actuated by electroactive polymers," *IEEE Robot. Autom. Lett.*, vol. 1, no. 1, pp. 391–398, Jan. 2016.
[20] M. S. Malekzadeh, S. Calinon, D. Bruno, and D. G. Caldwell, "Learning by imitation with the STIFF-FLOP surgical robot: A biomimetic approach inspired by octopus movements," *Robot. Biomimetics*, vol. 1, no. 1, p. 13, 2014.
[21] V. Vavourakis, D. Bampasakis, A. Kazakidi, N. Pateromichelakis, J. A. Ekaterinaris, and D. P. Tsakiris, "Generation of primitive behaviors for non-linear hyperelastic octopus-inspired robotic arm," in *Proc. 4th Int. Conf. Biomed. Robot. Biomechatronics (BioRob)*, Jun. 2012, pp. 725–730.
[22] I. Seleem, H. El-Hussieny, and S. Assal, "Development of a demonstration-guided motion planning for multi-section continuum robots," in *Proc. IEEE Int. Conf. Syst., Man, Cybern. (SMC)*, Oct. 2018, pp. 333–338.
[23] I. A. Seleem, H. El-Hussieny, and S. F. M. Assal, "Motion planning for continuum robots: A learning from demonstration approach," in *Proc. 27th IEEE Int. Symp. Robot Hum. Interact. Commun. (RO-MAN)*, Aug. 2018, pp. 868–873.
[24] B. A. Jones and I. D. Walker, "Kinematics for multisection continuum robots," *IEEE Trans. Robot.*, vol. 22, no. 1, pp. 43–55, Feb. 2006.
[25] A. Amouri, A. Zaatri, and C. Mahfoudi, "Dynamic modeling of a class of continuum manipulators in fixed orientation," *J. Intell. Robotic Syst.*, vol. 91, nos. 3–4, pp. 413–424, 2018.
[26] H. Mochiyama and T. Suzuki, "Dynamical modelling of a hyper-flexible manipulator," in *Proc. 41st SICE Annu. Conf. (SICE)*, vol. 3, Aug. 2002, pp. 1505–1510.
[27] H. Mochiyama and T. Suzuki, "Kinematics and dynamics of a cable-like hyper-flexible manipulator," in *Proc. Int. Conf. Robot. Autom. (ICRA)*, vol. 3, Sep. 2003, pp. 3672–3677.
[28] E. Tatlicioglu, I. D. Walker, and D. M. Dawson, "Dynamic modelling for planar extensible continuum robot manipulators," in *Proc. IEEE Int. Conf. Robot. Autom. (ICRA)*, Apr. 2007, pp. 1357–1362.
[29] V. Falkenhahn, T. Mahl, A. Hildebrandt, R. Neumann, and O. Sawodny, "Dynamic modeling of bellows-actuated continuum robots using the Euler–Lagrange formalism," *IEEE Trans. Robot.*, vol. 31, no. 6, pp. 1483–1496, Dec. 2015.
[30] V. Falkenhahn, T. Mahl, A. Hildebrandt, R. Neumann, and O. Sawodny, "Dynamic modeling of constant curvature continuum robots using the Euler–Lagrange formalism," in *Proc. IEEE/RSJ Int. Conf. Intell. Robots Syst. (IROS)*, Sep. 2014, pp. 2428–2433.
[31] M. Dehghani and S. A. A. Moosavian, "Dynamics modeling of a continuum robotic arm with a contact point in planar grasp," *J. Robot.*, vol. 2014, Nov. 2014, Art. no. 308283.
[32] F. Baumgart, "Stiffness—An unknown world of mechanical science?" *Injury*, vol. 31, no. 2, pp. 14–23, 2000.
[33] A. Ude, A. Gams, T. Asfour, and J. Morimoto, "Task-specific generalization of discrete and periodic dynamic movement primitives," *IEEE Trans. Robot.*, vol. 26, no. 5, pp. 800–815, Oct. 2010.
[34] A. Ude, B. Nemec, T. Petrić, and J. Morimoto, "Orientation in Cartesian space dynamic movement primitives," in *Proc. Int. Conf. Robot. Autom. (ICRA)*, May/Jun. 2014, pp. 2997–3004.
[35] D.-H. Park, H. Hoffmann, P. Pastor, and S. Schaal, "Movement reproduction and obstacle avoidance with dynamic movement primitives and potential fields," in *Proc. 8th IEEE-RAS Int. Conf. Humanoid Robots*, Dec. 2008, pp. 91–98.
[36] B. Kenwright, "A beginners guide to dual-quaternions: What they are, how they work, and how to use them for 3D character hierarchies," in *Proc. 20th Int. Conf. Comput. Graph., Vis. Comput. Vis. WSCG Commun.*, 2012, pp. 1–13.
[37] S. Kucuk and Z. Bingul, "Robot kinematics: Forward and inverse kinematics," in *Industrial Robotics: Theory, Modelling and Control*. Rijeka, Croatia: InTech, 2006.
[38] B. Siciliano, L. Sciavicco, S. Chiaverini, P. Chiacchio, L. Villani, and F. Caccavale, "Jacobian-based algorithms: A bridge between kinematics and control," in *Proc. Special Celebratory Symp.*, 2003, pp. 4–35.
[39] J.-J. E. Slotine and W. Li, *Applied Nonlinear Control*, vol. 199. Englewood Cliffs, NJ, USA: Prentice-Hall, 1991.
[40] F. L. Lewis, D. M. Dawson, and C. T. Abdallah, *Robot Manipulator Control: Theory and Practice*. Boca Raton, FL, USA: CRC Press, 2003.
[41] T. Hu and Z. Lin, "Composite quadratic Lyapunov functions for constrained control systems," *IEEE Trans. Autom. Control*, vol. 48, no. 3, pp. 440–450, Mar. 2003.
[42] W. Shang and S. Cong, "Nonlinear computed torque control for a high-speed planar parallel manipulator," *Mechatronics*, vol. 19, no. 6, pp. 987–992, Sep. 2009.

IBRAHIM A. SELEEM received the B.Sc. degree in industrial electronics and control engineering from the Faculty of Electronic Engineering at Menouf, Menoufia University, Egypt, in 2012, and the M.Sc. degree in mechatronics and robotics engineering from the Egypt-Japan University of Science and Technology (E-JUST), Alexandria, Egypt, in 2017, where he is currently pursuing the Ph.D. degree with the Mechatronics and Robotics Engineering Department, since September 2017. He has been a Visiting Research Fellow with the Modern Mechanical Engineering Department, Faculty of Science and Engineering, Waseda University, Tokyo, Japan, since March 2019. His research interests include soft robots, teleoperation, human–robot interaction, and the motion planning of humanoid robots.

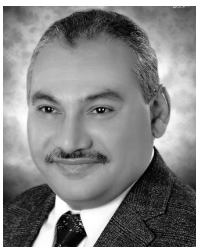

SAMY F. M. ASSAL received the B.Sc. and M.Sc. degrees in mechanical power engineering from Alexandria University, Alexandria, Egypt, in 1989 and 1997, respectively, and the Ph.D. degree in robotics and intelligent systems from Saga University, Saga, Japan, in March 2006. He is currently a Professor of mechatronics and robotics with the Department of Production Engineering and Mechanical Design, Faculty of Engineering, Tanta University, Tanta, Egypt. He is also a Professor of mechatronics and robotics with the Department of Mechatronics and Robotics Engineering, Egypt-Japan University of Science and Technology (E-JUST), Egypt. His current research interests include the dynamics and control of nonlinear systems, intelligent control systems, neural network control and fuzzy control with their applications to redundant manipulators, parallel manipulators and mobile robots, the applications of parallel manipulators to medical assistive devices, machine tools and pot seedlings transplanting, and mechatronic systems design such as smart actuator-based hand rehabilitation systems.

HIROYUKI ISHII received the B.S. and M.S. degrees in mechanical engineering and the Ph.D. degree in biomedical engineering from Waseda University, Japan, in 2002, 2004, and 2007, respectively. He is currently an Associate Professor with the Department of Modern Mechanical Engineering, Waseda University. His research interest includes interactive robots which induce behavior modifications on humans and animals. He received the Young Scientists' Prize, The Commendation for Science and Technology by the Minister of Education, Culture, Sports, Science and Technology, Japan, in 2018.

HAITHAM EL-HUSSIENY received the B.Sc. degree in electronics and communication engineering from the Faculty of Engineering at Shoubra, Benha University, Egypt, in 2007, and the M.Sc. and Ph.D. degrees in mechatronics and robotics engineering from the Egypt-Japan University of Science and Technology (E-JUST), Alexandria, Egypt, in 2013 and 2016, respectively. Since August 2019, he has been a Senior Research Fellow with the University of Salford, Manchester, U.K. He is currently an Assistant Professor of robotics with the Electrical Engineering Department, Faculty of Engineering at Shoubra, Benha University (currently on leave). His research interests include soft robots, soft haptics, teleoperation, human–robot interaction, and applied intelligence.